Efficiency of a Quantum Otto Heat Engine Operating under a Reservoir at Effective Negative Temperatures

Rogério J. de Assis,[1] Taysa M. de Mendonça,[2] Celso J. Villas-Boas,[2] Alexandre M. de Souza,[3] Roberto S. Sarthour,[3] Ivan S. Oliveira,[3] and Norton G. de Almeida[1]

[1]*Instituto de Física, Universidade Federal de Goiás, 74.001-970, Goiânia—GO, Brazil*
[2]*Departamento de Física, Universidade Federal de São Carlos, 13565-905, São Carlos, São Paulo, Brazil*
[3]*Centro Brasileiro de Pesquisas Físicas, Rua Dr. Xavier Sigaud 150, 22290-180 Rio de Janeiro, Rio de Janeiro, Brazil*

We perform an experiment in which a quantum heat engine works under two reservoirs, one at a positive spin temperature and the other at an effective negative spin temperature, i.e., when the spin system presents population inversion. We show that the efficiency of this engine can be greater than that when both reservoirs are at positive temperatures. We also demonstrate the counterintuitive result that the Otto efficiency can be beaten only when the quantum engine is operating in the finite-time mode.

Negative temperature is one of the most exciting current topics in contemporary physics, being subject to skepticism and criticism in the scientific community. This topic emerged in 1951 when Purcell [1] first produced spin states with inverted population and considered the possibility of describing them as states at negative spin temperatures. In 1956, Ramsey [2] studied these states theoretically, considering them as states of thermodynamic equilibrium, and discussed the consequences on the bases of thermodynamics arising from the incorporation of negative temperatures, one of them being the need for modifications of thermodynamics laws. After more than 60 years since the experiment carried out by Purcell [1], another experiment [3,4] involving negative temperatures called attention to this topic, which has triggered a discussion on the definition of equilibrium entropy in statistical mechanics, or the "Boltzmann vs Gibbs entropy" issue [5–15]. Recently, H. Struchtrup [16] studied this subject from a different point of view by considering states at negative temperatures as nonequilibrium states, referring to them as temperature unstable states or states with apparent negative temperatures, thus, keeping unchanged the bases of thermodynamics. Although the concept of negative temperature has proven controversial, fortunately, it is not necessary to enter this debate to investigate a heat engine operating in such environments. Indeed, both equilibrium and nonequilibrium reservoirs have already been considered in previous works, see, for instance, Refs. [17–26]. However, here, we will use the nonequilibrium approach discussed in Ref. [16], referring to states with apparent negative temperatures as states at effective negative temperatures.

Classical heat engines convert thermal resources into work, which is maximized for reversible operations in which the entropy production vanishes. In the quantum realm, both the engine and the reservoirs can be composed of finite-dimensional systems. Different from the classical case, quantum engines can be prepared in physical states without classical analogues [26]. These quantum states, in which the working substance as well the reservoirs can be prepared, give rise to an out-of-equilibrium scenario where it is legitimate to expect improved heat engines as compared to their classical analogs. Indeed, it was recently demonstrated that the use of squeezed thermal reservoirs allows for thermal engines of greater efficiencies [22,24]. As a special example, the quantum Otto heat engine (QOHE) consists of two isochoric thermalization branches, one with a cold and another with a hot thermal reservoir in which the Hamiltonian is fixed, and two other branches, in which the system is disconnected from the thermal reservoirs and evolves unitarily [17–21,23,27–30]. Recently, QOHE operating with reservoirs at positive temperatures was experimentally performed in the nuclear magnetic resonance (NMR) context and fully characterized in the finite-time operation mode [25]. This experiment demonstrated that the quantumness of the work substance is not enough to have gain in efficiency. Furthermore, the work extracted from a QOHE is limited to the same amount of work extracted from a classical Otto engine, and besides, the maximum work is extracted only at the quasistatic operation mode [25].

In this Letter, we show a proof-of-concept implementation of a QOHE that operates under a thermal reservoir at a positive spin temperature and another one at an effective negative spin temperature. As far as we know, our experiment is the first one to investigate quantum heat engines with a reservoir at negative effective temperatures. As a consequence of this new approach, we obtained extremely innovative and counterintuitive results as higher efficiency than the Otto limit and, for some set of parameters, the faster the process, the higher the efficiency.
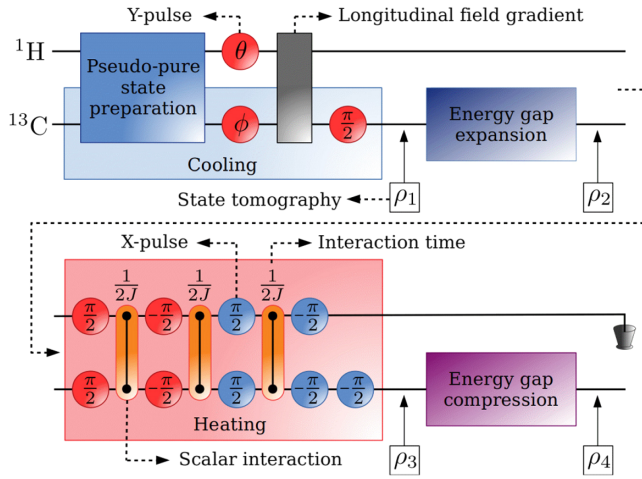
FIG. 1. Circuit to QOHE implementation protocol. The blue (red) circles represent transverse rf pulses in the x (y) direction that produce rotations by the angles displayed into the circle. The θ and ϕ angles were adjusted to produce the desired populations (see the main text).

To implement the QOHE we employed a ^{13}C-labeled CHCl$_3$ liquid sample diluted in Acetone-D6 and a 500 MHz Varian NMR spectrometer. Because of dilution, each chloroform molecule (CHCl$_3$) can be seen as an independent two-qubit system, named ^{13}C and ^{1}H nuclear spins. The coupling interaction between ^{13}C and ^{1}H nucleus is $J = 215.1$ Hz and their Larmor frequencies are $\nu_L^H = 500$ and $\nu_L^C = 125$ MHz. As in Ref. [25], the spin $1/2$ of the ^{13}C nucleus is the working medium, and the spin $1/2$ of the ^{1}H nucleus plays the role of the hot thermal reservoir. The experiments were performed at room temperature. Radio frequency pulses allow manipulating the ^{13}C and ^{1}H spin populations separately and, therefore, can be used to prepare different Boltzmann distributions. In the timescale of the experiment, these distributions remain basically unchanged due to the long thermal relaxation time, which in NMR is associated with the spin lattice relaxation occurring in a characteristic time τ_1 ($\tau_1^H \sim 7.4$ s and $\tau_1^C \sim 11.3$ s). The four strokes of the quantum Otto cycle are indicated below and the respective simplified experimental protocol is shown in Fig. 1.

(i) Cooling stroke. At first, using spatial average techniques employed by radio frequency (rf) and gradient fields, the ^{13}C nuclear spin is prepared in a pseudothermal state equivalent to $\rho_1 = e^{-\beta_{\rm cold} H_{\rm cold}}/Z_{\rm cold}$, where $\beta_{\rm cold}$ is the cold inverse effective spin temperature, $H_{\rm cold}$ is the Hamiltonian, and $Z_{\rm cold}$ is the partition function. The cold inverse effective spin temperature has the form $\beta_{\rm cold} = 1/k_B T_{\rm cold}$, with k_B being the Boltzmann's constant and $T_{\rm cold}$ the cold effective spin temperature. The Hamiltonian is given by $H_{\rm cold} = -\frac{1}{2}h\nu_{\rm cold}\sigma_x^C$, with h being the Planck's constant, $\nu_{\rm cold}$ a frequency to be specified, and $\sigma_{x,y,z}^C$ the Pauli matrices.

(ii) Expansion stroke. In this stage, from time $t = 0$ to $t = \tau$, the time-modulated rf field resonant with the ^{13}C nuclear spin drives the working medium Hamiltonian according to $H_{\rm exp}(t) = -\frac{1}{2}h\nu(t)[\cos(\pi t/2\tau)\sigma_x^C + \sin(\pi t/2\tau)\sigma_y^C]$, with $\nu(t) = \nu_{\rm cold}[1 - (t/\tau)] + \nu_{\rm hot}(t/\tau)$, in a rotating frame at the frequency ν_L^C. The rf-field intensity is adjusted so that $\nu_{\rm cold} = 2.0$ and $\nu_{\rm hot} = 3.6$ kHz, thus, expanding the energy gap. The driving time τ will be varied into the interval from 100 to 400 μs. This time is much shorter than the decoherence scales, which has the order of seconds, implying that we can describe the driving process as almost unitary [25,31]. Therefore, the *expansion stroke* drives the working medium Hamiltonian to $H_{\rm exp}(\tau) = -\frac{1}{2}h\nu_{\rm hot}\sigma_y^C \equiv H_{\rm hot}$ and unitarily evolves the ^{13}C nuclear spin state to $\rho_2 = U_{\tau,0}\rho_1 U_{\tau,0}^\dagger$, where $U_{\tau,0}$ stands for the unitary evolution operator.

(iii) Heating stroke. Here, the ^{13}C nuclear spin thermalizes at a hot inverse spin temperature $\beta_{\rm hot}$. The themalization is achieved by emulating the heat exchange between the working system and the bath using the ^{1}H nuclear spin as an auxiliary system, which is previously prepared in a pseudothermal state with inverse spin temperature $\beta_{\rm hot}$. This thermalization process is effectively achieved by applying a sequence of suitable rf pulses and free evolution between the nuclei under the scalar interaction $H_J = \frac{1}{4}hJ\sigma_z^C\sigma_z^H$, as sketched in Fig. 1. At the end of this stage, the ^{13}C nuclear spin state is in the Gibbs state $\rho_3 = e^{-\beta_{\rm hot} H_{\rm hot}}/Z_{\rm hot}$.

(iv) Compression stroke. At last, this stage is accomplished by reversing the protocol adopted in the above expansion stroke, such that the Hamiltonian is $H_{\rm comp}(t) = -H_{\rm exp}(\tau - t)$. This process is unitary, and at the end the ^{13}C nuclear spin state is $\rho_4 = V_{\tau,0}\rho_3 V_{\tau,0}^\dagger$, where $V_{\tau,0} = U_{\tau,0}^\dagger$.

The inverse temperature $\beta_{\rm cold(hot)}$ of the ^{13}C nuclear spin can be adjusted by means of the population of its excited state $p_{\rm cold(hot)}^+$ according to the relation

$$\beta_{\rm cold(hot)} = \frac{1}{h\nu_{\rm cold(hot)}}\ln\left(\frac{1 - p_{\rm cold(hot)}^+}{p_{\rm cold(hot)}^+}\right), \qquad (1)$$

where $p_{\rm cold(hot)}^+ = \langle +_{\rm cold(hot)}|\rho_{1(3)}|+_{\rm cold(hot)}\rangle$, with $|+_{\rm cold(hot)}\rangle$ being the eigenstate of the Hamiltonian $H_{\rm cold(hot)}$ with a positive eigenvalue. As can be seen from Eq. (1), $p_{\rm cold(hot)}^+ \in [0, 0.5)$ corresponds to $\beta_{\rm cold(hot)}$ positive, while $p_{\rm cold(hot)}^+ \in (0.5, 1]$ corresponds to $\beta_{\rm cold(hot)}$ negative. In turn, $p_{\rm cold}^+$ is adjusted by rf and gradient fields, as already mentioned in the cooling stroke, and $p_{\rm hot}^+$ by adjusting the population of the excited state of the ^{1}H nuclear spin, also using rf and gradient fields. In our experiment, see Fig. 1, ϕ was held fixed, corresponding to $p_{\rm cold}^+ = 0.261 \pm 0.004$, whereas θ was varied so that $p_{\rm hot}^+ \in (0.5, 1]$. The population $p_{\rm cold(hot)}^+$ is obtained by tomography of states $\rho_{1(3)}$ [32].

The successive repetition of the procedure (i) to (iv) above is equivalent to running successive cycles of the QOHE. Also, as each experimental realization of the protocol indicated in Fig. 1 involves spatial averages on a diluted liquid sample containing about 10^{17} noninteracting molecules, each experimental result presents an average over many copies of a single molecular spin engine [33,34]. All measurements in our experiment refer to a single realization of the protocol described in Fig. 1.

It is worthwhile to mention that the finite time, necessary to accomplish the expansion and compression stages, is responsible for transitions between the instantaneous eigenstates of the ^{13}C nuclear spin Hamiltonian. These transitions result in entropy production, which introduces irreversibility into the QOHE, causing the poor performance on thermal engines operating under thermal reservoirs at positive temperatures [25,35,36]. Surprisingly, as shown below, when the QOHE works under one thermal reservoir at a positive spin temperature and the other at an effective negative spin temperature, the finite-time operation mode improves the performance of the QOHE.

To understand our experimental results, first, we theoretically analyze the efficiency of the QOHE previously described and, in the following, we show the results obtained from our experiment. The first quantities we are interested in are the average net work $\langle W \rangle$ performed by the QOHE and the average heat $\langle Q_{\text{hot}} \rangle$ absorbed from the hot thermal reservoir, which is all the heat absorbed by the implemented QOHE.

After a straightforward calculation, using the information contained in the four strokes of the QOHE, together with the constraints $\beta_{\text{cold}} > 0$ and $\beta_{\text{hot}} < 0$ ($\beta_{\text{hot}} = -|\beta_{\text{hot}}|$), we obtain (see Supplemental Material [37]

$$\langle W \rangle = -\frac{h}{2}(\nu_{\text{hot}} - \nu_{\text{cold}})\left[\tanh\left(\frac{1}{2}\beta_{\text{cold}}h\nu_{\text{cold}}\right)\right.$$
$$\left. + \tanh\left(\frac{1}{2}|\beta_{\text{hot}}|h\nu_{\text{hot}}\right)\right] + h\xi\left[\nu_{\text{hot}}\tanh\left(\frac{1}{2}\beta_{\text{cold}}h\nu_{\text{cold}}\right)\right.$$
$$\left. - \nu_{\text{cold}}\tanh\left(\frac{1}{2}|\beta_{\text{hot}}|h\nu_{\text{hot}}\right)\right] \tag{2}$$

and

$$\langle Q_{\text{hot}} \rangle = \frac{h}{2}\nu_{\text{hot}}\left[\tanh\left(\frac{1}{2}\beta_{\text{cold}}h\nu_{\text{cold}}\right) + \tanh\left(\frac{1}{2}|\beta_{\text{hot}}|h\nu_{\text{hot}}\right)\right]$$
$$- \xi h\nu_{\text{hot}}\tanh\left(\frac{1}{2}\beta_{\text{cold}}h\nu_{\text{cold}}\right), \tag{3}$$

where $\xi = |\langle \pm_{\text{hot}}|U_{\tau,0}|\mp_{\text{cold}}\rangle|^2 = |\langle \pm_{\text{cold}}|V_{\tau,0}|\mp_{\text{hot}}\rangle|^2$ is the transition probability between the eigenstates $|\mp_{\text{cold}}\rangle$ and $|\pm_{\text{hot}}\rangle$. According to our convention, in order to extract work from the QOHE, we must have $\langle W \rangle < 0$. From Eq. (2), this implies

$$\xi < \frac{(\nu_{\text{hot}} - \nu_{\text{cold}})[\tanh\left(\frac{1}{2}\beta_{\text{cold}}h\nu_{\text{cold}}\right) + \tanh\left(\frac{1}{2}|\beta_{\text{hot}}|h\nu_{\text{hot}}\right)]}{2|\nu_{\text{hot}}\tanh\left(\frac{1}{2}\beta_{\text{cold}}h\nu_{\text{cold}}\right) - \nu_{\text{cold}}\tanh\left(\frac{1}{2}|\beta_{\text{hot}}|h\nu_{\text{hot}}\right)|}, \tag{4}$$

with $\nu_{\text{hot}}\tanh\left(\frac{1}{2}\beta_{\text{cold}}h\nu_{\text{cold}}\right) - \nu_{\text{cold}}\tanh\left(\frac{1}{2}|\beta_{\text{hot}}|h\nu_{\text{hot}}\right) \neq 0$. In the case where $\nu_{\text{hot}}\tanh\left(\frac{1}{2}\beta_c h\nu_{\text{cold}}\right) - \nu_{\text{cold}}\tanh\left(\frac{1}{2}|\beta_{\text{hot}}|h\nu_{\text{hot}}\right) = 0$, as can be seen in Eq. (2), the QOHE performs work regardless the value of ξ. The conditionality for extracting work from the QOHE is graphically shown in the red and blue regions of Fig. 2(a). The red region indicates the set of parameters where QOHE operates as a conventional heat engine, therefore, with efficiency $\eta < \eta_{\text{Otto}} \equiv 1 - \nu_{\text{cold}}/\nu_{\text{hot}}$, while the blue region, on the other hand, displays the set of parameters ξ for which efficiency beats that of a conventional QOHE, i.e., $\eta \geq \eta_{\text{Otto}}$, as will be demonstrated later in the calculations. Note that there is a blank area in Fig. 2(a). In that region, the system does not work out as a heat engine. So, not all values of ξ allow us to have a heat engine for the region $\eta < \eta_{\text{Otto}}$. However, for the region where $\eta \geq \eta_{\text{Otto}}$, our system works out as a heat engine for all values of ξ. Figure 2(b) shows that the transition probability goes to zero when the driving time is increased, as expected by the quantum adiabatic theorem.

Since ξ contains all information about the speed at which the expansion and compression stages are performed, see Fig. 2(b), the contribution to the net work due to the finite-time realization of these stages lies on the term containing ξ in Eq. (2). Thus, ξ can be viewed as an adiabaticity parameter. Besides, this term can be identified with the total inner friction, which is the difference between the average net work considering actual processes and the average net work considering ideal (adiabatic) processes [35]. In this way, the total inner friction is related to the nonadiabaticity of the expansion and compression processes and, therefore, related to the entropy production [35]. When we consider one of the thermal reservoirs with
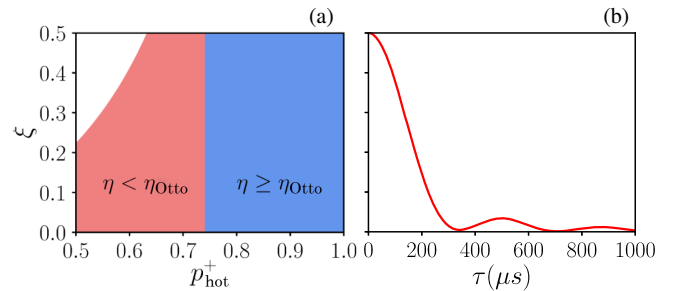

FIG. 2. (a) Transition probability ξ versus excited state population p_{hot}^+ of the ^{13}C nuclear spin. Red and blue regions separate the regimes where efficiency is improved (blue) as compared with the conventional QOHE (red). (b) Transition probability ξ versus expansion or compression (assumed the same) time τ. Note that, due to the protocol adopted here, this transition probability is upper limited by $\xi = 1/2$.

negative temperature, surprisingly, ξ may contribute to the increase of the extracted net work, as can be seen directly in Eq. (2), unlike what happens when we consider only thermal reservoirs with positive temperatures [25]. If the other QOHE parameters are properly adjusted, the faster the expansion and compression processes are performed, the greater the contribution of this parameter ξ to the extracted work, since ξ increases with the shortening of time interval, see Fig. 2(b). It is important to note that the increase of the extracted work with the decrease of time causes the power of the QOHE to increase, which is a motivating factor for the implementation of a QOHE operating under the effective negative temperature thermal reservoir. Indeed, this is the main message from Fig. 2(b).

Now, we can look at the QOHE efficiency. From Eqs. (2) and (3), the QOHE efficiency, which is given by $\eta = -\langle W \rangle / \langle Q_{\text{hot}} \rangle$, can be written as (see Supplemental Material [37])

$$\eta = 1 - \frac{\nu_{\text{cold}}}{\nu_{\text{hot}}} \left(\frac{1 - \xi \mathcal{F}}{1 - \xi \mathcal{G}} \right), \tag{5}$$

where

$$\mathcal{F} = \frac{\tanh\left(\frac{1}{2}|\beta_{\text{hot}}|h\nu_{\text{hot}}\right)}{\tanh\left(\frac{1}{2}\beta_{\text{cold}}h\nu_{\text{cold}}\right) + \tanh\left(\frac{1}{2}|\beta_{\text{hot}}|h\nu_{\text{hot}}\right)}, \tag{6}$$

and

$$\mathcal{G} = \frac{\tanh\left(\frac{1}{2}\beta_{\text{cold}}h\nu_{\text{cold}}\right)}{\tanh\left(\frac{1}{2}\beta_{\text{cold}}h\nu_{\text{cold}}\right) + \tanh\left(\frac{1}{2}|\beta_{\text{hot}}|h\nu_{\text{hot}}\right)}. \tag{7}$$

Equation (5) shows that, when $\xi = 0$, we have $\eta = 1 - \nu_{\text{cold}}/\nu_{\text{hot}} \equiv \eta_{\text{Otto}}$, which is the upper limit for the efficiency of Otto cycles operating under thermal reservoirs both at positive spin temperatures. Strikingly, as in the case of extracted net work, now $\xi \neq 0$ can contribute to the increase of the QOHE efficiency, causing it to overtake η_{Otto}. By analyzing Eqs. (5)–(7), it is possible to show that $\beta_{\text{cold}}\nu_{\text{cold}} < |\beta_{\text{hot}}|\nu_{\text{hot}}$ implies $\eta < \eta_{\text{Otto}}$ while $\beta_{\text{cold}}\nu_{\text{cold}} \geq |\beta_{\text{hot}}|\nu_{\text{hot}}$ implies $\eta \geq \eta_{\text{Otto}}$, corresponding to the red and blue regions of Fig. 2.

Our experimental results are shown in Figs. 3(a)–3(b), where the efficiency of the QOHE is plotted against the population of the excited state for several driving times τ ranging from 100 to 400 μs. The efficiency is obtained by means of the average energy of the ^{13}C nuclear spin after each stroke, see the Supplemental Material [37], where the Hamiltonians H_{cold} and H_{hot} are used together with the nuclear spin states ρ_i, $i = 1, 2, 3, 4$, obtained by tomography (see Supplemental Material [37]). Dashed lines are for our theoretical results; dots are the experimental measurements. Note, in Fig. 3(a), the intersection point corresponding to the transition point from $\eta < \eta_{\text{Otto}}$ to $\eta \geq \eta_{\text{Otto}}$. This point is also shown in Fig. 2(a). It is
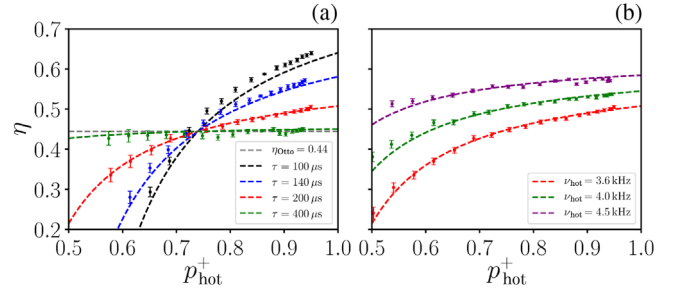

FIG. 3. Efficiency (η) against the population (p_{hot}^+) of the excited state. Dashed lines are the theoretical results while the dots are the experimental measurements. (a) η vs p_{hot}^+ for several finite operation times, keeping the frequency ratio fixed ($\nu_{\text{cold}} = 2.0$ kHz and $\nu_{\text{hot}} = 3.6$ kHz). The intersection of the curves happens at the transition point between the regimes $\eta < \eta_{\text{Otto}}$ and $\eta \geq \eta_{\text{Otto}}$. (b) η vs p_{hot}^+ for different frequency ratios $\nu_{\text{cold}}/\nu_{\text{hot}}$, with $\nu_{\text{cold}} = 2$ kHz. The driving time is fixed in $\tau = 200$ μs.

important to note that the faster the expansion and compression steps (small driving times τ), the greater the engine efficiency in the regime in which $\eta \geq \eta_{\text{Otto}}$. In fact, note that, to the right of the intersection point, the best efficiency occurs for $\tau = 100$ μs (black dashed line and dots). Also, since η increases with the decreasing of the ratio $\nu_{\text{cold}}/\nu_{\text{hot}}$, see Eq. (5), in Fig. 3(b), we show the efficiency against the population of the excited state, now for a fixed driving time $\tau = 200$ μs while varying this frequency ratio with $\nu_{\text{cold}} = 2$ kHz. Note that the smaller this ratio, the greater the efficiency, as expected. Therefore, we can use this ratio to improve the QOHE efficiency.

In conclusion, we experimentally performed a quantum Otto heat engine in the context of nuclear magnetic resonance by considering one of the two reservoirs being at effective negative spin temperature. Such fermionic reservoirs can be engineered, for example, by inverting the population of a huge nuclear hydrogen spin system. Thus, by weakly coupling a single nuclear carbon spin to this "sea" of nuclear spins of the hydrogen atoms, the engineered reservoir is able to invert the population of the main nuclear spin system (carbon nuclear spin) as if it were effectively coupled to a negative temperature reservoir [39]. Unlike previous works with classical and quantum heat engines, which operate with reservoirs at positive temperatures, our system provides a set of parameters in which the faster the processes are performed, the greater the efficiency of the engine, which we proved experimentally. In this way, our heat engine is not limited to adiabatic (slow) processes to obtain high efficiencies. Thus, while the efficiency of conventional Otto engines reaches the maximum $\eta_{\text{Otto}} = 1 - \nu_c/\nu_h$ when its expansion and compression processes occur reversibly, thus, in the limit of null output power, our implemented QOHE reaches $\eta = \eta_{\text{Otto}}$ and $\eta > \eta_{\text{Otto}}$ when its expansion and compression processes occur adiabatically and nonadiabatically, respectively. In addition, for a

QOHE operating under reservoirs at positive spin temperatures only, the nonadiabaticity as measured by the parameter $\xi = |\langle \pm_{\text{hot}}|U_{\tau,0}|\mp_{\text{cold}}\rangle|^2$ comes from the finite-time regime and is responsible for decreasing the engine efficiency. However, in our experiment, this parameter ξ can be used to increase the engine efficiency. Besides, our QOHE allows us to obtain efficiency superior to the Otto limit, also proven experimentally, remembering that we do not take into account the work of engineering the reservoir at effective negative temperature, following the same approach of previous works that show superior efficiencies for out of equilibrium reservoirs, like squeezed ones [22,24]. Finally, different from works in Ref. [40,41], where the energy is directly converted into mechanical work, our experiment consists in a proof of concept providing the efficiency and maximum work that can be obtained from our QOHE. Thus, the results presented here can trigger new investigations on quantum heat engines in out of equilibrium reservoirs and applications for effective negative temperature systems.

[1] E. M. Purcell and R. V. Pound, Phys. Rev. **81,** 279 (1951).
[2] N. F. Ramsey, Phys. Rev. **103,** 20 (1956).
[3] L. D. Carr, Science **339,** 42 (2013).
[4] S. Braun, J. P. Ronzheimer, M. Schreiber, S. S. Hodgman, T. Rom, I. Bloch, and U. Schneider, Science **339,** 52 (2013).
[5] J. Dunkel and S. Hilbert, Nat. Phys. **10,** 67 (2014).
[6] I. M. Sokolov, Nat. Phys. **10,** 7 (2014).
[7] S. Hilbert, P. Hänggi, and J. Dunkel, Phys. Rev. E **90,** 062116 (2014).
[8] M. Campisi, Phys. Rev. E **91,** 052147 (2015).
[9] L. Cerino, A. Puglisi, and A. Vulpiani, J. Stat. Mech. (2015) P12002.
[10] D. Frenkel and P. B. Warren, Am. J. Phys. **83,** 163 (2015).
[11] R. H. Swendsen and J.-S. Wang, Phys. Rev. E **92,** 020103 (R) (2015).
[12] J. Poulter, Phys. Rev. E **93,** 032149 (2016).
[13] R. H. Swendsen and J.-S. Wang, Physica (Amsterdam) **453A,** 24 (2016).
[14] E. Abraham and O. Penrose, Phys. Rev. E **95,** 012125 (2017).
[15] Y. Hama, W. J. Munro, and K. Nemoto, Phys. Rev. Lett. **120,** 060403 (2018).
[16] H. Struchtrup, Phys. Rev. Lett. **120,** 250602 (2018).
[17] H. T. Quan, Y.-x. Liu, C. P. Sun, and F. Nori, Phys. Rev. E **76,** 031105 (2007).
[18] J. Gemmer, M. Michel, and G. Mahler, *Quantum Thermodynamics: Emergence of Thermodynamic Behavior Within Composite Quantum Systems*, 2nd ed. (Springer-Verlag, Berlin, 2009).
[19] N. Linden, S. Popescu, and P. Skrzypczyk, Phys. Rev. Lett. **105,** 130401 (2010).
[20] J.-Q. Liao, H. Dong, and C. P. Sun, Phys. Rev. A **81,** 052121 (2010).
[21] D. Gelbwaser-Klimovsky, R. Alicki, and G. Kurizki, Phys. Rev. E **87,** 012140 (2013).
[22] J. Roßnagel, O. Abah, F. Schmidt-Kaler, K. Singer, and E. Lutz, Phys. Rev. Lett. **112,** 030602 (2014).
[23] R. Alicki and D. Gelbwaser-Klimovsky, New J. Phys. **17,** 115012 (2015).
[24] J. Klaers, S. Faelt, A. Imamoglu, and E. Togan, Phys. Rev. X **7,** 031044 (2017).
[25] J. P. S. Peterson, T. B. Batalhão, M. Herrera, A. M. Souza, R. S. Sarthour, I. S. Oliveira, and R. M. Serra, arXiv:1803.06021.
[26] F. Tacchino, A. Auffèves, M. F. Santos, and D. Gerace, Phys. Rev. Lett. **120,** 063604 (2018).
[27] R. Alicki, J. Phys. A **12,** L103 (1979).
[28] E. Geva and R. Kosloff, J. Chem. Phys. **96,** 3054 (1992).
[29] T. D. Kieu, Phys. Rev. Lett. **93,** 140403 (2004).
[30] A. Roulet, Entropy **20,** 973 (2018).
[31] T. B. Batalhão, A. M. Souza, L. Mazzola, R. Auccaise, R. S. Sarthour, I. S. Oliveira, J. Goold, G. De Chiara, M. Paternostro, and R. M. Serra, Phys. Rev. Lett. **113,** 140601 (2014).
[32] G. M. Leskowitz and L. J. Mueller, Phys. Rev. A **69,** 052302 (2004).
[33] A. Abragam, *The Principles of Nuclear Magnetism* (Clarendon Press, Oxford, 1961).
[34] I. Oliveira, R. Sarthour, T. Bonagamba, E. Azevedo, and J. C. C. Freitas, *NMR Quantum Information Processing*, 1st ed. (Elsevier Science, Amsterdam, 2007).
[35] F. Plastina, A. Alecce, T. J. G. Apollaro, G. Falcone, G. Francica, F. Galve, N. Lo Gullo, and R. Zambrini, Phys. Rev. Lett. **113,** 260601 (2014).
[36] S. Cakmak, F. Altintas, and O. E. Mustecaplioglu, Eur. Phys. J. D **71,** 75 (2017).
[37] See Supplemental Material at http://link.aps.org/supplemental/10.1103/PhysRevLett.122.240602 for more details, which includes Refs. [21,32,38].
[38] X. Wang, C.-S. Yu, and X. Yi, Phys. Lett. A **373,** 58 (2008).
[39] T. M. de Mendonça, R. J. de Assis, A. M. de Souza, R. S. Sarthour, I. S. Oliveira, N. G. de Almeida, and C. J. Villas-Boas (to be published).
[40] J. Roßnagel, S. T. Dawkins, K. N. Tolazzi, O. Abah, E. Lutz, F. Schmidt-Kaler, and K. Singer, Science **352,** 325 (2016).
[41] D. von Lindenfels, O. Gräb, C. T. Schmiegelow, V. Kaushal, J. Schulz, F. Schmidt-Kaler, and U. G. Poschinger, arXiv:1808.02390.